

# Functionalized TiO<sub>2</sub> Nanotubes as Three-Dimensional Support for Loading Au@Pd Nanoparticles: Facile Preparation and Enhanced Materials for Electrochemical Sensor

Xianlan Chen<sup>1,2,3</sup>, Na Wu<sup>1</sup>, Guowei Zhang<sup>1</sup>, Shaoping Feng<sup>1</sup>, Keqiang Xu<sup>1</sup>, Wei Liu<sup>1</sup>, Haibo Pan<sup>2,3,\*</sup>

<sup>1</sup> School of Science, Honghe University, Mengzi, Yunnan 661100, China

<sup>2</sup> Fujian Key Lab of Medical Instrument & Pharmaceutical Technology, Yishan Campus, Fuzhou University, Fuzhou, Fujian 350002, China

<sup>3</sup> College of Chemistry and Chemical Engineering, Qishan Campus, Fuzhou University, Fuzhou, Fujian 350108, China

\*Corresponding author: Tel +86-591-22866127; Fax: +86-591-22866127; e-mail: \*E-mail:

[hbpan@fzu.edu.cn](mailto:hbpan@fzu.edu.cn), [13489086418@163.com](mailto:13489086418@163.com)

Received: 13 September 2016 / Accepted: 28 October 2016 / Published: 12 December 2016

---

A new composite nanostructure made of unique TiO<sub>2</sub>-based nanotubes (TiO<sub>2</sub>NTs) and coating 3-Aminopropyltrimethoxysilane (APTMS) anchor Au@Pd nanoparticles (Au@Pd NPs) has been demonstrated. APTMS covalent bonding of its functional silane groups onto the surface of hydrophilic TiO<sub>2</sub>NTs crystals, meanwhile APTMS acted as a linker, which provided metal-ligand bonding and hydrogen bonding interaction with Au@Pd NPs, resulting in the formation of Au@Pd NPs/f-TiO<sub>2</sub>NTs hybrid nanostructures. The resulting Au@Pd NPs/f-TiO<sub>2</sub>NTs hybrid nanostructures were characterized by SEM, TEM and Nitrogen adsorption-desorption isotherms and the results suggest the existence of the uniform distribution of Au@Pd NPs on the TiO<sub>2</sub>NTs surface with the help of APTMS. Moreover, the hybrid nanostructures were used as a promising catalyst in nonenzymatic electrochemical sensor because of its satisfactory or even enhanced electrocatalytic properties from both Au@Pd NPs and TiO<sub>2</sub>NTs. The electrochemical results indicate that as-prepared Au@Pd NPs/f-TiO<sub>2</sub>NTs hybrid nanostructures modified glassy carbon electrode (GCE) exhibits high electrocatalytic activity toward H<sub>2</sub>O<sub>2</sub> at low potential, the detection limit for H<sub>2</sub>O<sub>2</sub> were found to be 2×10<sup>-8</sup> M (S/N=3).

---

**Keywords:** TiO<sub>2</sub> nanotubes, APTMS, Au@Pd NPs/f-TiO<sub>2</sub>NTs hybrid nanostructures, Nonenzymatic electrochemical sensor, H<sub>2</sub>O<sub>2</sub>

## 1. INTRODUCTION

Ordered amine-functionalized nanomaterials have received considerable attention in recent years due to their numerous potential applications in adsorption, catalysis, separations and

biomolecules immobilization [1, 2]. Intensive ongoing research effort is devoted to the development of various aminosilanes and experimental functionalizing procedures, the goal being to grow homogeneous amine-functionalized nanomaterials, in order to further enable its widespread applications. The amino centers of aminopropylalkoxysilanes are generally used in various applications as coupling agents to immobilize different kinds of transition metal and noble metal nanoparticles on the surface of solid substrates (e.g., Si [3,4], SiO<sub>2</sub> and TiO<sub>2</sub> [5]). Researchers pointed out that these functionalized hybrid materials combined with the properties of various functional nanomaterials to achieve excellent catalytic activity and stability, which will play an important role in wider range of applications [6,7]. Base on these advantages, it is worthy to develop such multifunctional hybrid nanostructures attaching certain metal nanoparticles onto TiO<sub>2</sub> nanotubes.

There are some reports about the design and preparation of amine-functionalized hybrid nanostructures, especially the design of multifunctional noble metal nanoparticles (MNPs) supported on 1D nanomaterials, which have found many promising applications especially in electrochemical sensor [8,9], Li-ion batteries [10] and catalysis [11] for their unique properties. As an important family of amine-functionalized hybrid nanomaterials, functionalized TiO<sub>2</sub> hybrid nanostructures have been considered as a good photocatalyst or electrocatalyst candidate, because of the important optical and electronic properties, facile and environment friendly synthesis, non-toxicity and tunable size, it is useful for catalyst support, sensors, and so on [12,13]. More significantly, TiO<sub>2</sub> nanotubes (TiO<sub>2</sub>NTs) with high length-to-diameter ratio, pore volume and large specific surface area that can significantly increase the number of reaction sites and can remarkably enhance the absorption of nanomaterials such as Au [14], Au-Pd [15] and AgCu [12]. More interestingly, synthesis of TiO<sub>2</sub>NTs coaxial nanocables has attracted more attention due to TiO<sub>2</sub>NTs as a good supporting substrate can effectively prevent MNPs from aggregation and enhance their stability, which has been proved as an effective way to combine the unique electronic and mechanical properties of the supports, with the size- and shape-dependent physicochemical properties of MNPs [16]. Recent studies have also shown that entrapping MNPs in an active matrix (TiO<sub>2</sub>) improves the electrocatalytic activity and stability to a great extent due to the TiO<sub>2</sub>NTs's promising structural attributes including tubular inner pores and metal oxide properties [17]. Furthermore, MNPs present on the surface of TiO<sub>2</sub>NTs can induce additional electronic states in the band gap of TiO<sub>2</sub> thereby inhibiting the possibility of the recombination of the electron-hole pairs, resulting in the quicker charge transfer abilities and catalytic activity [18]. As a result, considerable efforts have been directed toward covalently or noncovalently attaching certain MNPs onto TiO<sub>2</sub>NTs and constructing the corresponding multifunctional hybrid nanostructures [7].

With regard to MNPs were immobilized on TiO<sub>2</sub>NTs, multimetallic nanoparticles structures are attractive materials, which exhibit better catalytic properties than their monometallic counterparts because of their composition-dependent optical, catalytic, electronic and magnetic properties [19]. It also has been reported that multimetallic nanoparticles modified electrodes have exhibited higher electrocatalytic activities for the detection of some small molecules such as methanol [20] and glucose [21] than single nanoparticles. Among the various bimetallic nanoparticles, the synergistic effects of the addition of Pd to Au in enhancing the overall catalytic activity, selectivity and stability of the catalyst [22,23]. More interestingly, unusual shape Au@Pd bimetallic nanostructures can use as an outstanding catalyst effectively increase the active sites and electrochemically active surface area, and

efficiently accelerate the electron transfer between catalyst and target molecules leading to an extraordinary electrochemical result [24, 25]. Inspired by above considerations, searching a simple and relatively inexpensive method for preparing amino-functionalized MNPs/TiO<sub>2</sub>NTs hybrid nanostructures are of great importance in nanotechnology.

There are some reports about the design and preparation of TiO<sub>2</sub>NTs functionalized by MNPs, which typically involve impregnation or sol-gel-based processes [26], sol technique [27], sonochemistry and light illumination [28]. Despite these successes in preparing MNPs/TiO<sub>2</sub> hybrid nanostructures, most of the sequential methods involve complicated procedures or rigorous conditions. In the present study, we developed a facile functionalization of TiO<sub>2</sub>NTs (f-TiO<sub>2</sub>NTs) by 3-aminopropyltrimethoxysilane (APTMS), aimed at the preparation of chemically modified nanotube surface capable of binding Au@Pd NPs, forming Au@Pd NPs/f-TiO<sub>2</sub>NTs coaxial hybrid nanostructures. APTMS are widely used coupling agents for solid-based materials because of their bifunctional nature, which lies in the fact that there are many possible ways for it to interact with surface silanol/silanolate groups, via hydrogen bonds, electrostatic attractions and siloxane bonds [29]. Nucleophilicity of -NH<sub>2</sub> groups in aminosilanes is taken advantage of in promoting adhesion in glass-resin composites, i.e., glassy carbon electrode (GCE). Herein, APTMS react with the hydroxyl groups for self-assembling amine functionality on the surface of TiO<sub>2</sub>NTs, forming surface-functionalized TiO<sub>2</sub>NTs, which is negatively charged in alkaline conditions and offers a versatile solid support for oppositely charged Au@Pd nanostructures. In this modified process, constructing Au@Pd NPs/f-TiO<sub>2</sub>NTs hybrid nanostructures using homogeneous TiO<sub>2</sub>NTs as a spacer has obvious advantages.

Hydrogen peroxide (H<sub>2</sub>O<sub>2</sub>) plays a significant role in the chemical, food, environmental and pharmaceutical industries as an oxidizing, bleaching and sterilizing agent [30]. However, at high concentrations, H<sub>2</sub>O<sub>2</sub> causes irritation to the eyes and skin, and affects human health [31]. Therefore, the determination of H<sub>2</sub>O<sub>2</sub> is not only related to the increased awareness of the environmental hazards but the need for safer procedures [32]. Electrochemical sensing of H<sub>2</sub>O<sub>2</sub> is one of the most promising approaches to monitor H<sub>2</sub>O<sub>2</sub>. To date, the application of Au@Pd NPs/f-TiO<sub>2</sub>NTs coaxial hybrid nanoclusters as high-performance electrocatalysts for constructing a H<sub>2</sub>O<sub>2</sub> electrochemical sensor has rarely been explored. Thus the modified electrodes based on Au@Pd NPs/f-TiO<sub>2</sub>NTs hybrid nanostructures were detected to H<sub>2</sub>O<sub>2</sub> in 0.1 M phosphate buffer solution (pH 7.4) in this literature. Moreover, the structure-activity correlations for the prepared hybrid nanocatalysts were systematically investigated by various characterizations.

## 2. EXPERIMENTAL

### 2.1. Reagents

TiO<sub>2</sub> powder (P25, 70% anatase and 30% rutile) was purchased from Degussa, and their primary particle diameters were in the range of 30-50 nm. K<sub>2</sub>PdCl<sub>4</sub> and HAuCl<sub>4</sub>·4H<sub>2</sub>O were purchased from Sinopharm Chemical Reagent Co. Ltd. (Shanghai, China). 3-Aminopropyltrimethoxysilane (APTMS) and NaBH<sub>4</sub> were obtained from J&K Chemical Co. Ltd. H<sub>2</sub>O<sub>2</sub> was the product of Guangzhou Chemical Reagent Company (Guangzhou, China), and a fresh solution of H<sub>2</sub>O<sub>2</sub> was

prepared daily. The working solutions were prepared by diluting the stock solution with phosphate buffer solution (PBS) and water. A 0.1 M PBS consisting of  $\text{KH}_2\text{PO}_4$  and  $\text{Na}_2\text{HPO}_4$  was employed as the supporting electrolyte. All other chemicals used were of analytical reagent grade. Ultra-pure water was obtained with a Milli-Q plus water purification system (Millipore Co. Ltd., USA) (18 M $\Omega$ ).

## 2.2. Characterization techniques

All the electrochemical measurements including cyclic voltammetry (CV) and chronoamperometric experiments were performed using CHI 660B electrochemical workstation (CH Instrument Company, Shanghai, China). A counter electrode (a Pt wire), reference electrode (an Ag/AgCl electrode) and a working electrode (a modified glassy carbon electrode (GCE)) formed a three-electrode compartment cell, and all experiments were carried out at room temperature. Electrocatalytic  $\text{H}_2\text{O}_2$  reduction measurements were carried out in a 0.1 M PBS solution containing 0.5 mM  $\text{H}_2\text{O}_2$ . Surface morphologies of the samples across the entire substrate were characterized by field-emission scanning electron microscopy (FE-SEM, Nova Nano SEM 230, FEI, USA). The UV-vis spectra (Perkin-Elmer Lambda 900 USA), High-resolution transmission electron microscope (HRTEM) image was obtained using Tecnai G2 F20 S-TWIN, 200 kV (FEI Company, USA).  $\xi$ -potential value measurement was performed on Zeta Sizer3000 Laser Particle Size and Zeta Potential Tester (Malvern Corporation, UK) with the Au@Pd NPs in aqueous solution. Nitrogen adsorption-desorption isotherms were obtained using Autosorb-1 (Quantachrome Instruments, USA), and specific surface area was calculated by the Brunauer-Emmett-Teller (BET) method using adsorption isotherms.

## 2.3. Preparation of Au@Pd NPs/f-TiO<sub>2</sub>NTs hybrid nanostructures

Au@Pd NPs were prepared according to seed-mediated growth method, with Au nanoparticles as seeds and without any surfactant, where tens of small Pd nanoparticles (~3 nm) aggregated on gold seeds (~20 nm). These nanoparticles with positive charges were performed on zeta ( $\xi$ ) potential analyzer, and the  $\xi$ -potential is determined to be +51.8 mV [25].

Surface hydroxyl groups seem to be necessary for the formation of the alkoxy silane molecules on the TiO<sub>2</sub>NTs surfaces, thus TiO<sub>2</sub>NTs was prepared by hydrothermal method [33]. Most importantly, the post-thermal treatment of TiO<sub>2</sub>NTs avoid the elimination of surface OH group and to stabilize tube morphology [34], ensuring the methoxy groups of APTMS react with the native hydroxyl groups adorning the TiO<sub>2</sub>NTs surface [35], forming f-TiO<sub>2</sub>NTs, which is negatively charged in alkaline conditions (the  $\xi$ -potential was determined to be -17.6 mV (Fig.1), as a result of the hydrolyzation of APTMS and offers versatile solid supports for Au@Pd nanostructures. In brief, 0.05 g TiO<sub>2</sub>NTs and 20 mL ethanol were placed in a beaker equipped with magnetic stirring bars. In the second step, 200  $\mu\text{L}$  of APTMS was added to the above solution, followed by the addition of 2 mL of water and 2 mL of ammonia. In the third step, the resulting solution was stirred for more than 12 h and then centrifuged to remove the excess APTMS and further washed with ethanol and water for three times, respectively. Finally, the collected white precipitation was dissolved into 10 mL of water. It is crucial to preparation

of hybrid nanostructures with large-area high-quality while maintaining superior electrocatalytic activity and stability. Here, Au@Pd NPs/f-TiO<sub>2</sub>NTs hybrid nanostructures were synthesized by adding excess Au@Pd NPs (5 mL) to 0.5 mL of f-TiO<sub>2</sub>NTs, and then sonicated for 30 min. During the sonication process, f-TiO<sub>2</sub>NTs with more anchors can facilitate uniform dispersion of Au@Pd NPs. Finally, the hybrid nanostructures were centrifuged and washed 2-3 times with distilled water, and the purified Au@Pd NPs/f-TiO<sub>2</sub>NTs nanostructures were dispersed in 2 mL of water, which formed a gray, stable and homogeneous suspension that could stay stable for at least 1 month [36].

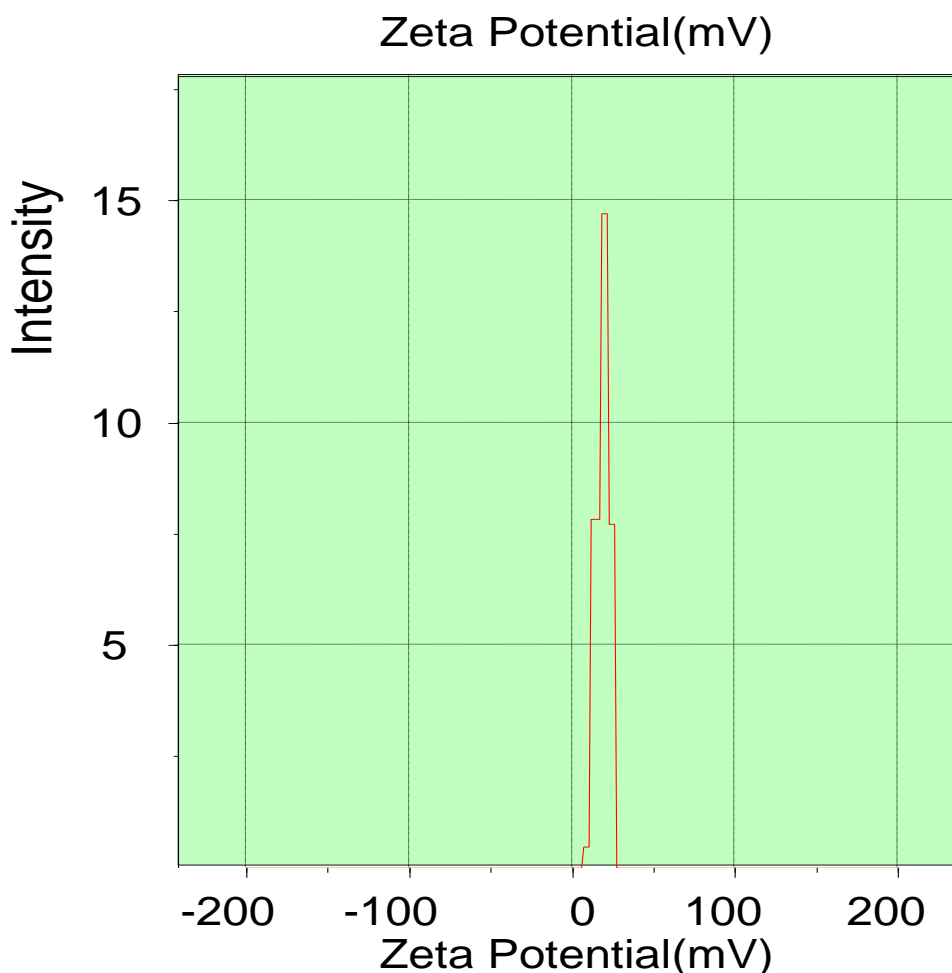


**Figure 1.** The  $\xi$ -potential of f-TiO<sub>2</sub> NTs in the neutral media solution.

#### 2.4. Preparation of the electrochemical sensor

Prior to preparation of electrochemical sensor, the clean GCE was polished to mirror smooth with alumina (under 0.3 and 0.05  $\mu\text{m}$  diameter) slurries, and subsequently washed by water and ultrasonicated in distilled water and ethanol bath. Finally, the electrode was dried under pure N<sub>2</sub>. The modified electrode was loaded with Au@Pd NPs/f-TiO<sub>2</sub>NTs hybrid nanostructures (10  $\mu\text{L}$ ) and dried under an infrared lamp. Thus a uniform film coated electrode (Au@Pd NPs/f-TiO<sub>2</sub>NTs/GCE) was obtained. The other modified electrodes as were fabricated through similar method.

### 3. RESULTS AND DISCUSSION

#### 3.1. Physicochemical Characterization

Obviously, APTMS played a crucial role in the formation of Au@Pd NPs/f-TiO<sub>2</sub>NTs hybrid nanocomposites, the accessibility of the amine functional groups in TiO<sub>2</sub>NTs and offers a versatile solid support for Au@Pd nanostructures was investigated by UV-vis spectra in Fig.2. UV-vis spectrum of f-TiO<sub>2</sub>NTs shows one absorption band around ~290 nm, which exhibited a blue shift compared with not functionalized TiO<sub>2</sub>NTs (Fig.2(a)), indicating the methoxy groups of APTMS reacted with the native hydroxyl groups adorning the TiO<sub>2</sub>NTs surface. It can be observed that a very pronounced gold characteristic peak at 510 nm is obtained while f-TiO<sub>2</sub>NTs support for Au nanoparticles (Fig.2(b)). Nevertheless, while tens of small Pd nanoparticles were aggregated on gold seeds, the intensity of the surface plasmon resonance peak of gold fades away (Fig.2(c)). Unlike the absorption characteristics of Au nanoparticles, Pd nanoparticles show a rather broad and strong absorption in the 200-800 nm region, which gradually increases toward the blue [37].

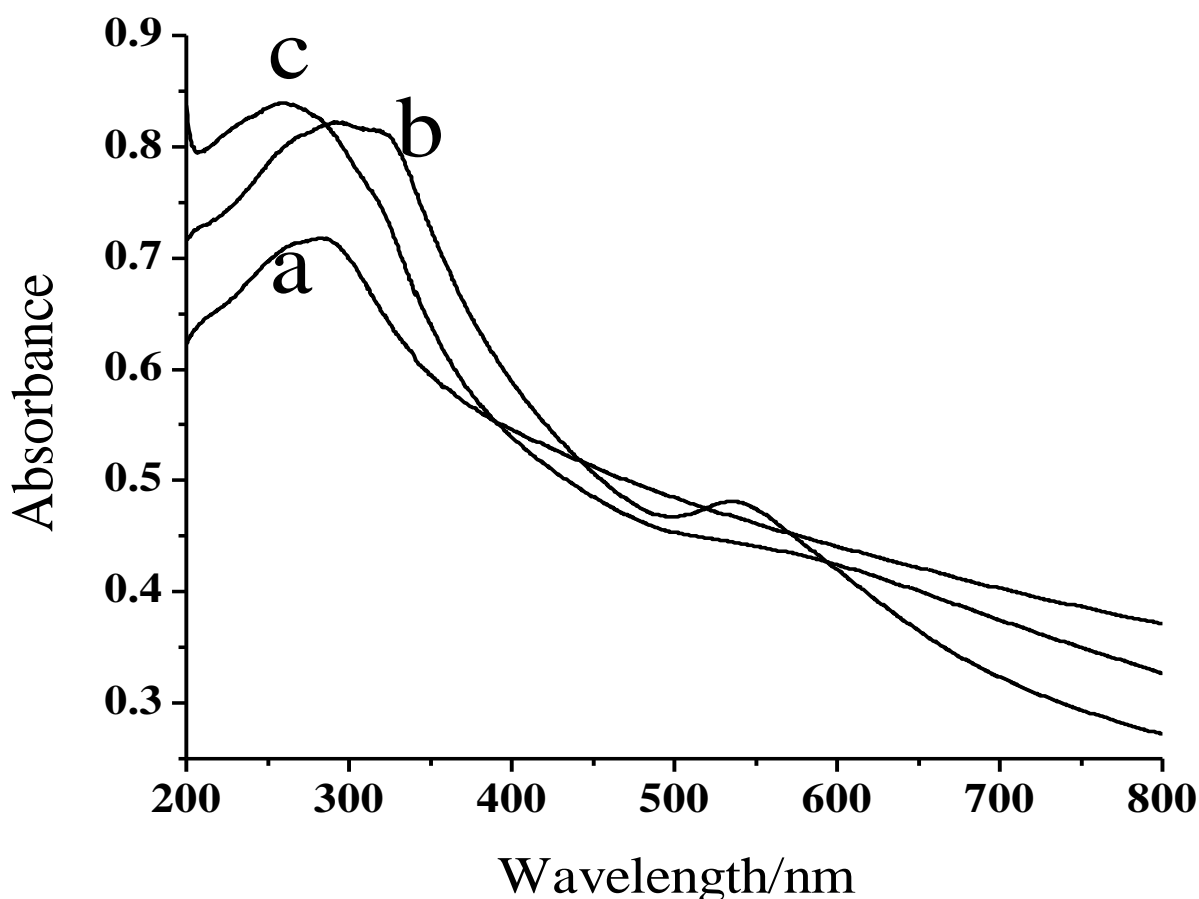


**Figure 2.** UV-vis spectrum of f-TiO<sub>2</sub>NTs (a), f-TiO<sub>2</sub>NTs-Au (b) and Au@Pd NPs/f-TiO<sub>2</sub>NTs hybrid nanostructures (c).

SEM images of TiO<sub>2</sub>NTs (Fig. 3) demonstrated that TiO<sub>2</sub>NTs have a length range of 2~3  $\mu\text{m}$  with a diameter of 30~50 nm and become crystalline upon annealing, and that the TiO<sub>2</sub>NTs were

loosely tangled together. The large number of cavities which appeared on the surface of the TiO<sub>2</sub>NTs confirmed their porous characteristic, consistent with the results of BET analysis shown below.

The HRTEM technique was applied to observe the deep nanostructure inside TiO<sub>2</sub>NTs. Fig. 4 a, b shows typical HRTEM images of the as-made TiO<sub>2</sub>NTs at different magnifications. In Fig. 4a, a great number of 1D open-ended TiO<sub>2</sub>NTs possessed long tubular structure with a wall thickness of about 2-3 nm and uniform inner diameters of about 25 nm could be observed. Due to the incomplete growth of the nanotubes, a small number of shorter TiO<sub>2</sub>NTs was obtained. Interesting, the TiO<sub>2</sub>NTs were open-ended, which can be observed more clearly in Fig. 4b, the formation mechanism is trititanate (Ti<sub>3</sub>O<sub>7</sub>)<sub>2</sub>-sheets may grow within the intermediate phase, caused by the reaction between NaOH and TiO<sub>2</sub> nanoparticles [38]. The nanosheets grow with an increasing tendency of curling, leading to the formation of nanotubes with open-ended. The as-obtained TiO<sub>2</sub>NTs arrays possess a larger surface area and one-dimensional channel, which can provide a higher number of accessible surface sites and a more rapid electron transportation resulting in superior electrochemical performance to H<sub>2</sub>O<sub>2</sub> reduction.

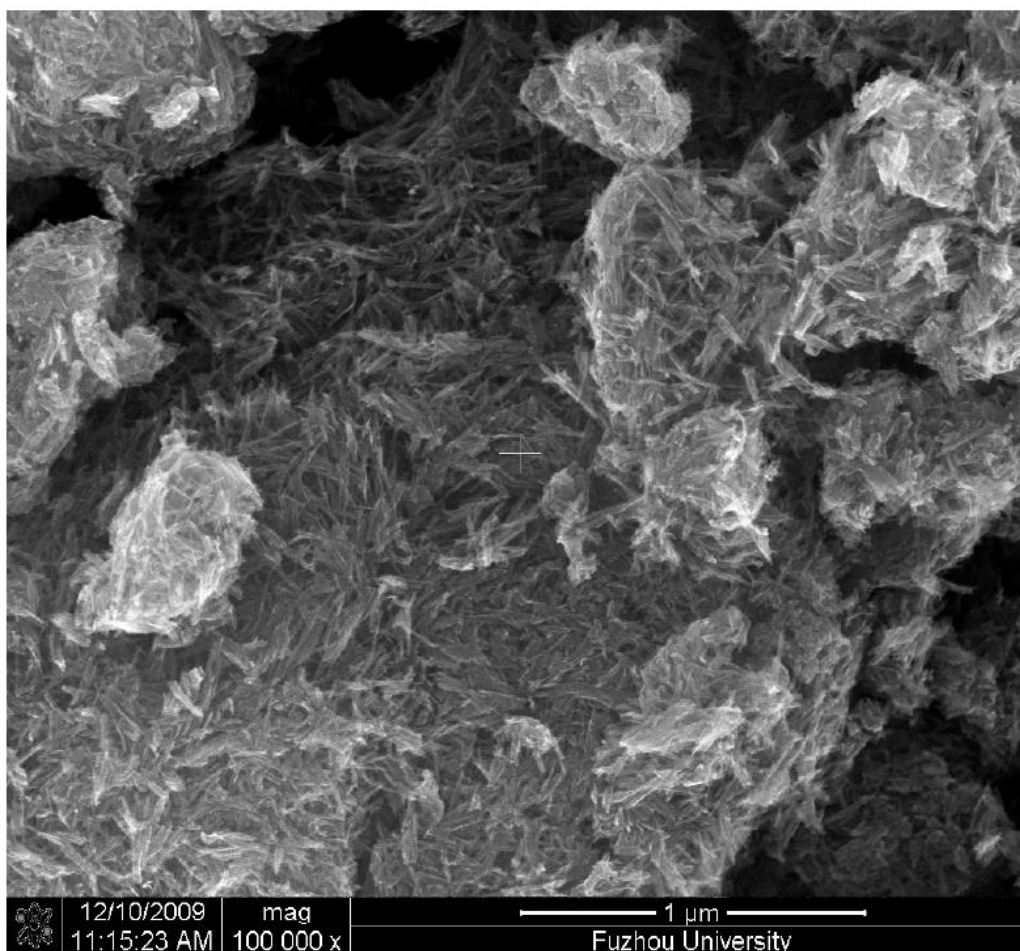


**Figure 3.** SEM images of TiO<sub>2</sub> nanotubes were prepared by hydrothermal method.

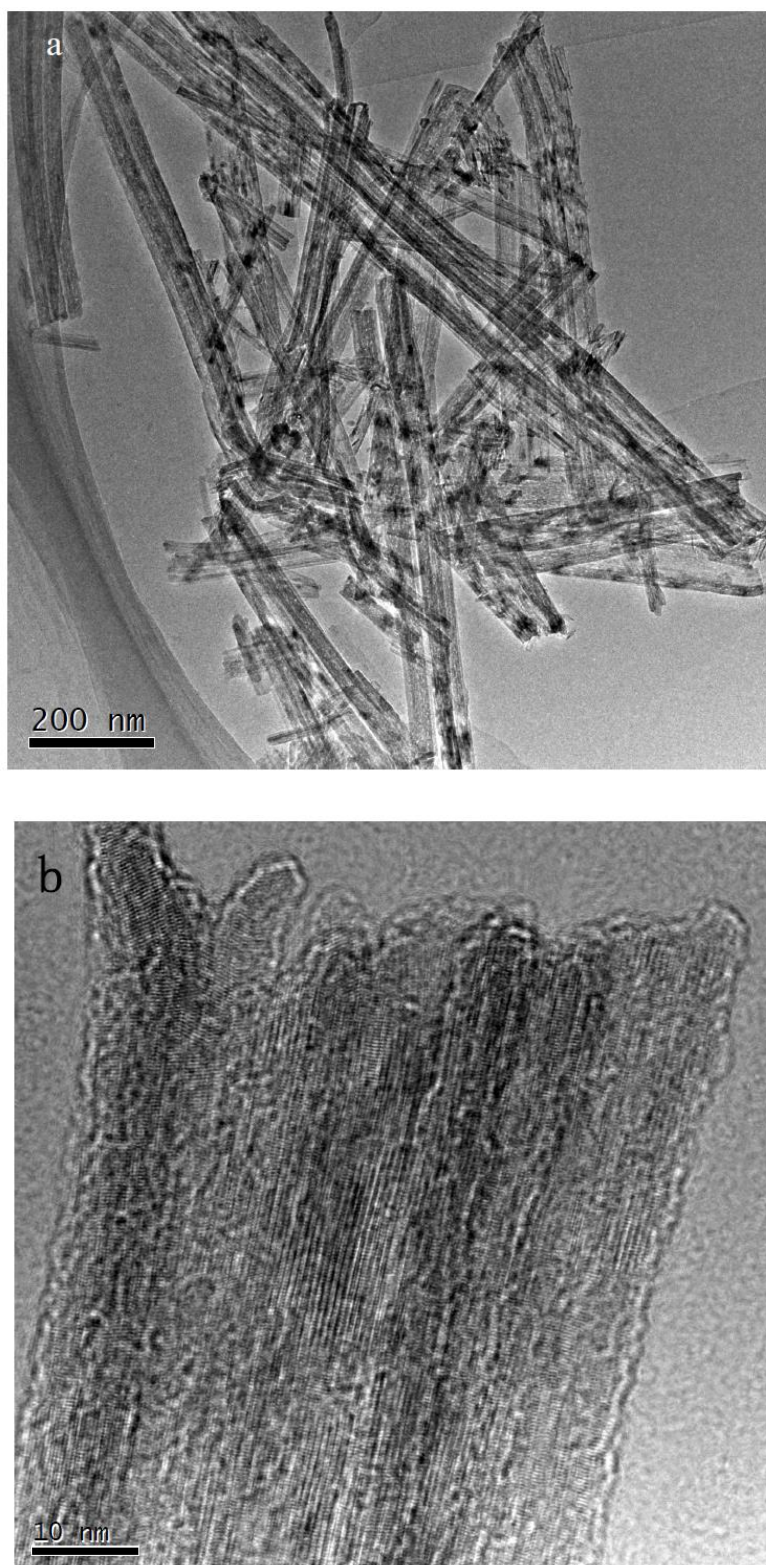
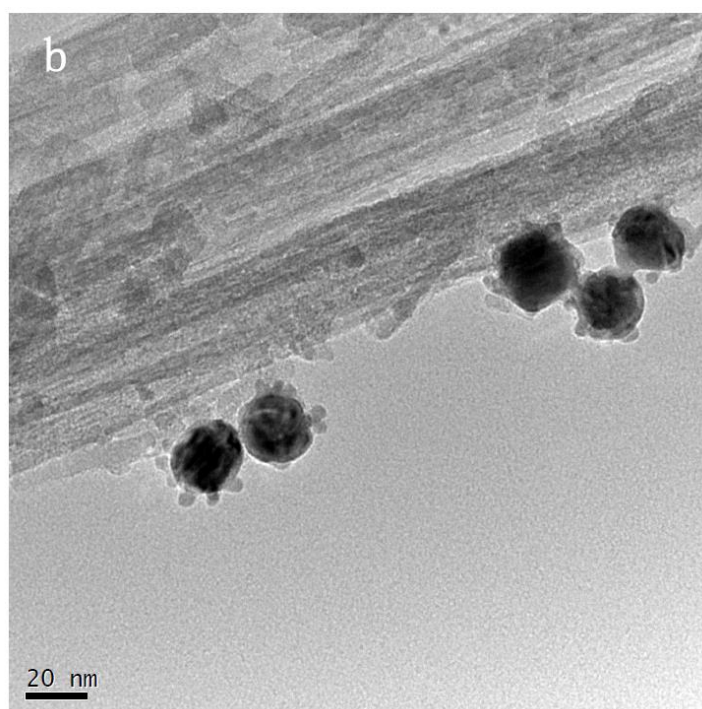
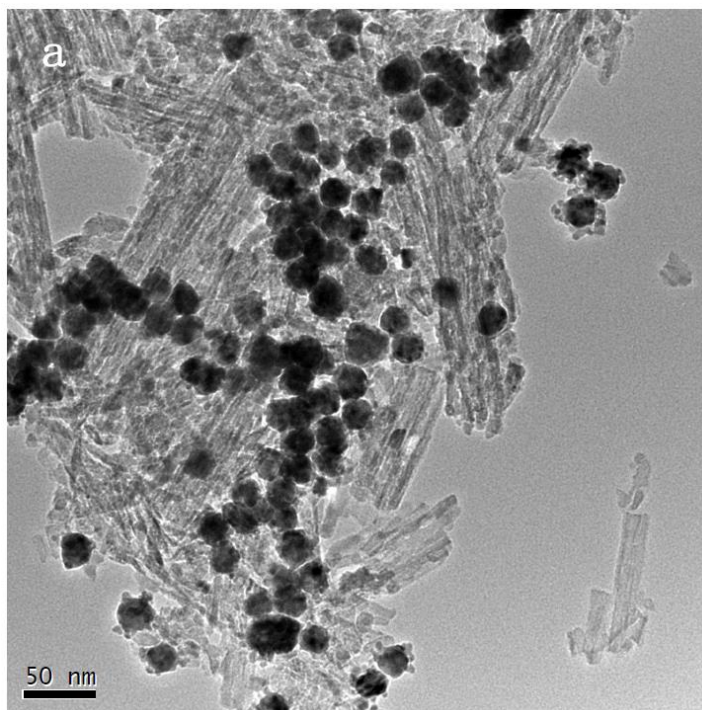


**Figure 4.** HRTEM image of TiO<sub>2</sub> nanotubes (a), open-ended TiO<sub>2</sub> nanotubes (b).

It is interesting to note that after functionalization with a -NH<sub>2</sub> group, f-TiO<sub>2</sub>NTs coaxial nanotubes could easily adsorb Au@Pd NPs. Fig. 5 shows the typical as-prepared structures composed of tubular amine-functionalized TiO<sub>2</sub>NTs and Au@Pd NPs, indicating that the Au@Pd NPs with sizes

of about ~25 nm had been completely anchor on f-TiO<sub>2</sub>NTs. Moreover, compared with TiO<sub>2</sub>NTs (Fig. 4), the f-TiO<sub>2</sub>NTs have a rougher surface due to APTMS. A high-magnification image (Fig. 5b) shows that very homogeneous APTMS layers are coated on the surface of the TiO<sub>2</sub>NTs, and Au@Pd NPs anchor on TiO<sub>2</sub>NTs through -NH<sub>2</sub> groups of APTMS.

A contrast difference in Au@Pd NPs with a darker center surrounded by a lighter edge is observed, confirming their core/shell structure.



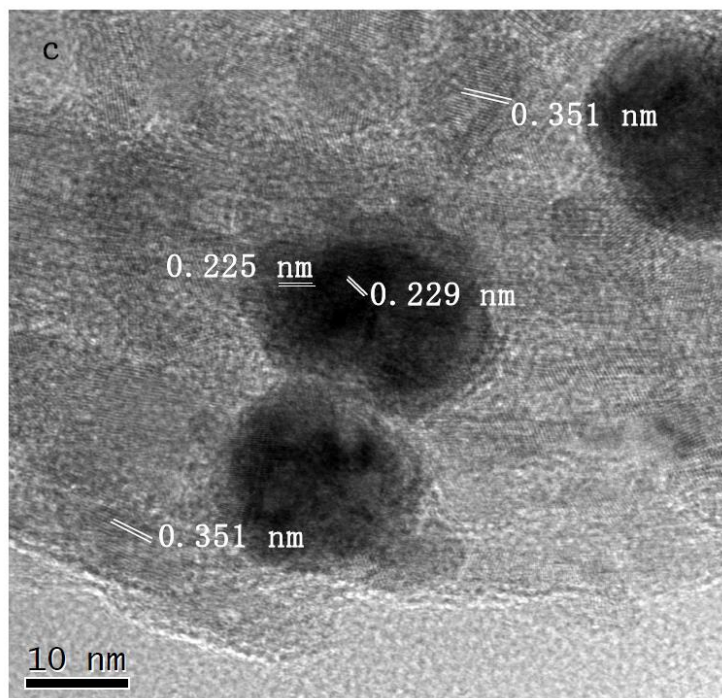


**Figure 5.** (a) TEM images of the Au@Pd NPs/f-TiO<sub>2</sub>NTs hybrid nanostructures. (b) An augmentation of Au@Pd NPs/f-TiO<sub>2</sub>NTs hybrid nanostructures. (c) HRTEM image displaying the lattice fringes of the Au@Pd NPs/f-TiO<sub>2</sub>NTs hybrid nanostructures.

An Au@Pd crystal phase appeared and showed good crystallinity in Fig. 5c, the inner core (Au) and external flower layer (Pd) have values of lattice spacing of 0.235 and 0.225 nm in Au@Pd NPs, corresponding to the mean value of the (111) planes of face-centered cubic (fcc) Au and Pd, respectively. The lattice spacing of 0.351 nm is assigned to (101) plane of anatase TiO<sub>2</sub>NTs. Because of the -NH<sub>2</sub> groups of APTMS anchor Au@Pd NPs with hydrogen bonds and metal-ligand coordination bonds, and the methoxy groups are available for the covalent linkage with abundant -OH groups from the surfaces of the TiO<sub>2</sub>NTs, there coaxial hybrid nanostructures can shorten the electronic transmission distance from the analyte to the surface of the modified electrode, thus enhancing significantly electrocatalytic active of the hybrid nanocatalysts.

TiO<sub>2</sub> nanoparticles (P25), TiO<sub>2</sub>NTs and Au@Pd NPs/f-TiO<sub>2</sub>NTs hybrid nanostructures were characterized by N<sub>2</sub> adsorption-desorption at -195 °C, as shown in Fig. 6. The N<sub>2</sub> adsorption-desorption isotherm of TiO<sub>2</sub>NTs and Au@Pd NPs/f-TiO<sub>2</sub>NTs hybrid nanostructures presented a type IV isotherm according to the IUPAC classification, displaying the porous characteristics of nanotubes. An adsorption-desorption hysteresis loop was observed at  $P/P_0 \approx 0.58$ , indicating capillary condensation inside the mesoporous TiO<sub>2</sub>NTs, which was in agreement with the TEM results. Due to excellent biocompatibility, ion-changeable ability, special geometry (porous structure) and high ratio of surface to volume, TiO<sub>2</sub>NTs can be used as an excellent carrier for quantitative loading of Au@Pd NPs to amplify the electrical catalytic signal, which leads to highly sensitive nonenzymatic sensor. After Au@Pd NPs were anchored to the surface of f-TiO<sub>2</sub>NTs, the BET surface area reduced from 184.9 to 160.6 m<sup>2</sup>/g, which is due to the f-TiO<sub>2</sub>NTs appear some aggregation after functionalization with APTMS. Correspondingly, the BET surface area of the raw material (P25) is only 53 m<sup>2</sup>/g,

indicating that TiO<sub>2</sub>NTs with high surface area and adsorption ability, providing favorable condition to support Au@Pd NPs.

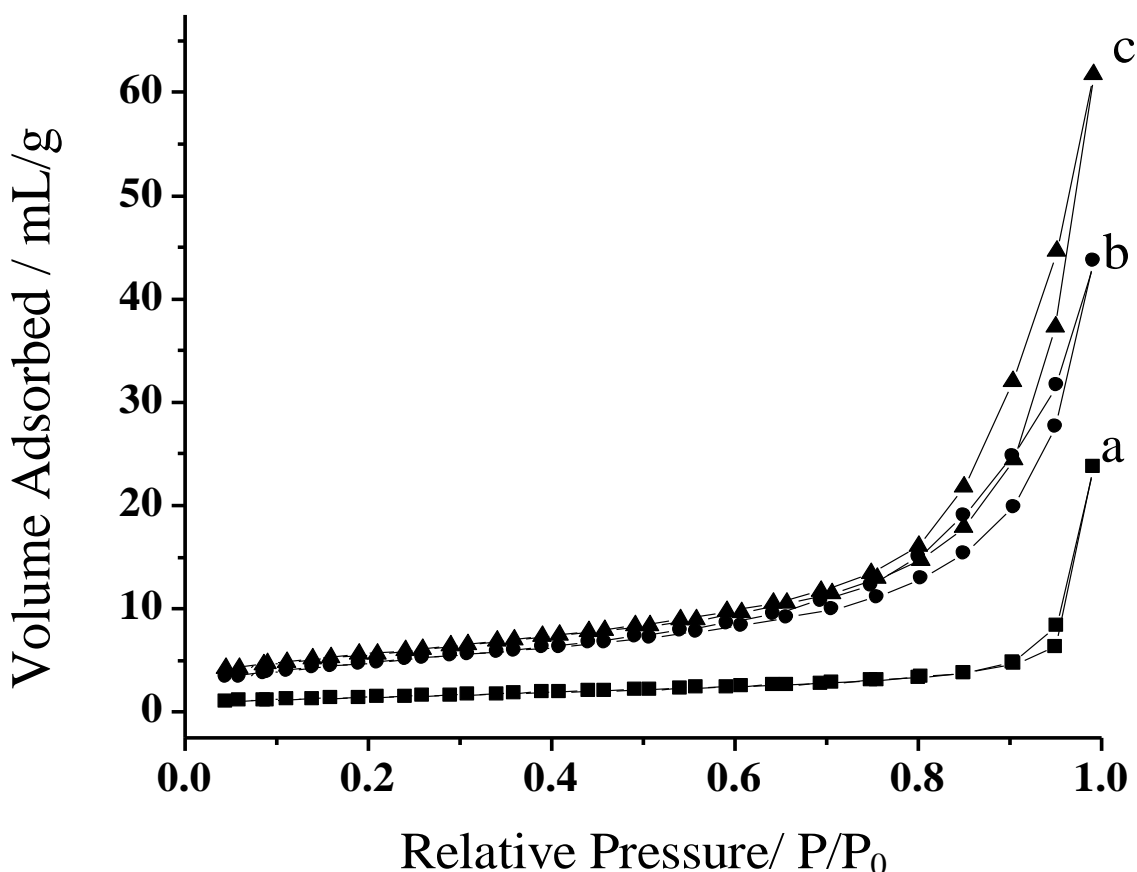


**Figure 6.** Isotherm of nitrogen adsorption-desorption at  $-195\text{ }^{\circ}\text{C}$  on the surface of TiO<sub>2</sub> nanoparticles (P25) (a), TiO<sub>2</sub>NTs (b) and Au@Pd NPs/f-TiO<sub>2</sub>NTs hybrid nanostructures (c).

### 3.2. Detection of Hydrogen Peroxide

The reliable, accurate and rapid determination of H<sub>2</sub>O<sub>2</sub> is practical important, and the present Au@Pd NPs/f-TiO<sub>2</sub>NTs/GCE provides a good opportunity to build a highly sensitive H<sub>2</sub>O<sub>2</sub> electrochemical sensor. Fig. 7 shows the CVs of bare GCE (line a) and GCEs modified by f-TiO<sub>2</sub>NTs (line b) and Au@Pd NPs/f-TiO<sub>2</sub>NTs nanocomposites (lines c) in presence of 0.5 mM H<sub>2</sub>O<sub>2</sub> in 0.1 M PBS (pH 7.0). It was observed that the Au@Pd NPs/f-TiO<sub>2</sub>NTs/GCE exhibits strong reduction current starting at around 0.25 V, and an obvious peak current (115  $\mu\text{A}$ ) occurs at 0.0 V while no reduction peaks of H<sub>2</sub>O<sub>2</sub> were observed at the bare GCE and f-TiO<sub>2</sub>NTs/GCE (line b), indicating that the Au@Pd NPs/f-TiO<sub>2</sub>NTs nanocomposites modified electrode showed well electrocatalytic activity toward H<sub>2</sub>O<sub>2</sub> reduction. In inset of Fig. 7, CVs measured using the Au@Pd NPs/f-TiO<sub>2</sub>NTs/GCE in the absence (d) and presence (c) of 0.5 mM H<sub>2</sub>O<sub>2</sub>. These results indicate that Au@Pd NPs can effectively choose and catalyze H<sub>2</sub>O<sub>2</sub> reduction on the electrode surface.

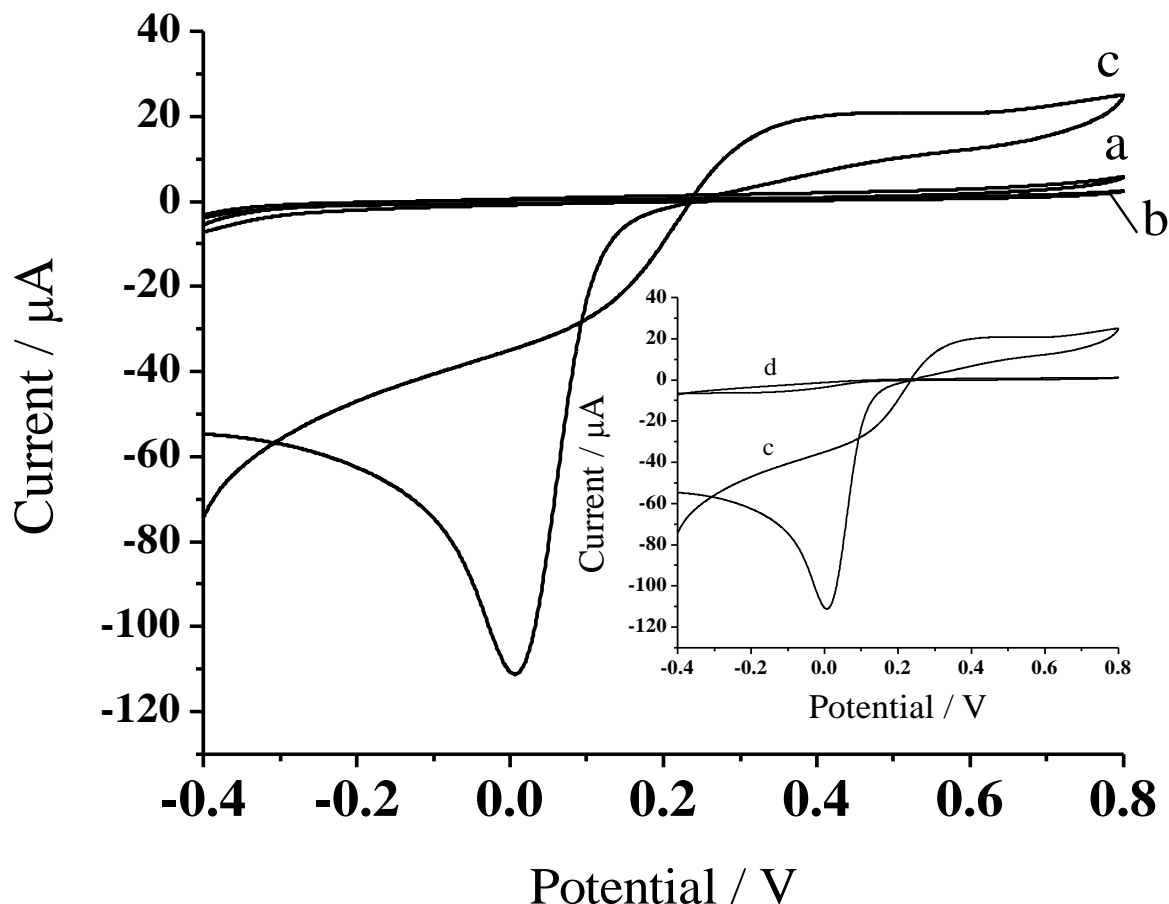


**Figure 7.** CVs obtained for the bare GCE (a) f-TiO<sub>2</sub>NTs/GCE (b) and Au@Pd NPs/f-TiO<sub>2</sub>NTs/GCE (c), immersed in 0.1 M 20 mL PBS (pH 7.4) containing 0.5 mM H<sub>2</sub>O<sub>2</sub> at the scan rate of 50 mV s<sup>-1</sup>. The inset is CVs of the Au@Pd NPs/f-TiO<sub>2</sub>NTs/GCE in the absence (d) and presence (c) of 0.5 mM H<sub>2</sub>O<sub>2</sub>, the scan rate at 50 mV s<sup>-1</sup>.

To investigate the reaction kinetics and the fast electron-transfer properties of the Au@Pd NPs/f-TiO<sub>2</sub>NTs hybrid nanocatalysts, the effect of scan rate on the reduction of H<sub>2</sub>O<sub>2</sub> at the Au@Pd NPs/f-TiO<sub>2</sub>NTs/GCE is shown in Fig. 8. As shown in Fig. 8, when the scan rates increase from 20 to 160 mV/s, the cathodic peak currents increase and the regression equation is  $I_p = -33.675 - 5.646 \times v^{1/2}$  with  $R^2 = 0.998$ . The peak currents increase linearly with the square root of the scan rate in the range of 20-160 mV/s, indicating that it was a diffusion controlled process.

To reveal the electrocatalytic activity of Au@Pd NPs/f-TiO<sub>2</sub>NTs nanocomposites toward the reduction of H<sub>2</sub>O<sub>2</sub>, the amperometric behavior of H<sub>2</sub>O<sub>2</sub> was investigated at Au@Pd NPs/f-TiO<sub>2</sub>NTs/GCE. Fig. 9 shows the *i-t* curve recorded at the Au@Pd NPs/f-TiO<sub>2</sub>NTs/GCE polarized at 0.0 V in 0.1 M stirring N<sub>2</sub>-saturated PBS (pH 7.4), where a H<sub>2</sub>O<sub>2</sub> stock solution was added. The low potential 0.0 V was chosen according to the results from Fig. 7, thus the risks of the electroactive interferences could be avoided. Upon addition of H<sub>2</sub>O<sub>2</sub>, the sensor responded rapidly to the substrate and achieved the steady-state current, indicating a fast amperometric response to the reduction of H<sub>2</sub>O<sub>2</sub>. The sensor had a linear relationship with the concentration of H<sub>2</sub>O<sub>2</sub> from 1×10<sup>-7</sup> to 5×10<sup>-4</sup> M with a correlation coefficient of 0.996, and the detection limit was found to be 2×10<sup>-8</sup> M (S/N=3). The

sensing performance between our present work and others regarding the performance of H<sub>2</sub>O<sub>2</sub> assays is presented in Table 1. With a wider linear response range, a relatively lower limit of detection and applied potential for H<sub>2</sub>O<sub>2</sub>, as-prepared Au@Pd NPs/f-TiO<sub>2</sub>NTs hybrid nanostructures can even be compared advantageously with respect to most others nonenzymatic H<sub>2</sub>O<sub>2</sub> sensors [30,39-43].

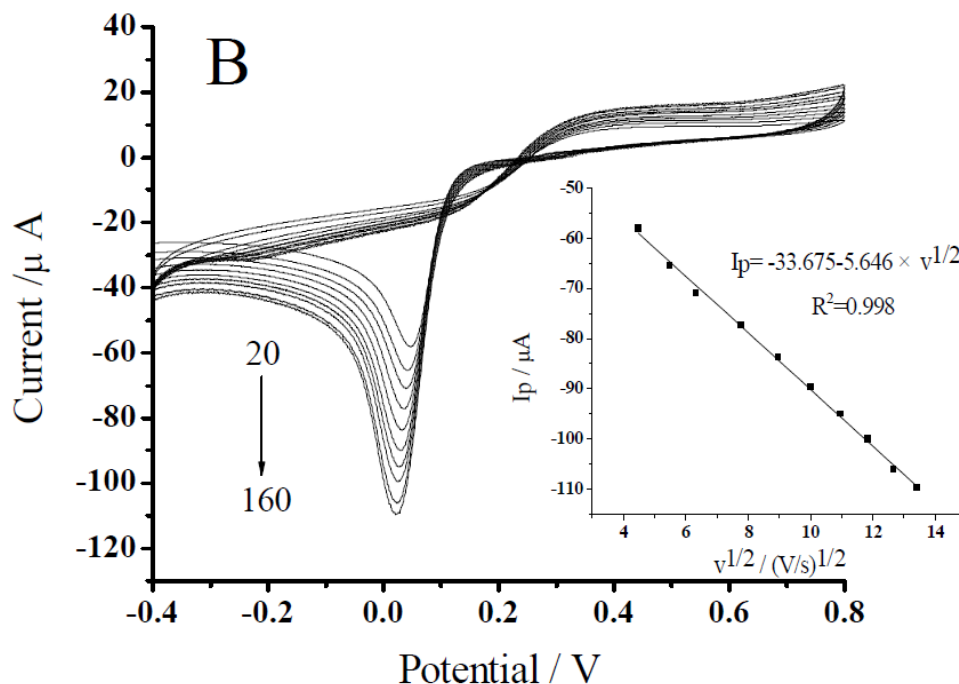


**Figure 8.** CVs of H<sub>2</sub>O<sub>2</sub> reduction at the Au@Pd NPs/f-TiO<sub>2</sub>NTs/GCE in 0.1 M 20 mL PBS (pH 7.4) containing 0.5 mM H<sub>2</sub>O<sub>2</sub> at different scan rates (from top to bottom: 20, 30, 40, 60, 80, 100, 120, 140 and 160 mV/s). The inset is the relationship between the reduction peak current ( $I_p$ ) and the scan rate (V/s).

**Table 1.** A comparison of this work with literature works regarding the performance of the H<sub>2</sub>O<sub>2</sub> assays.

Electrode material	Detection limit (μM)	Linear range	Sensitivity (μA mM <sup>-1</sup> cm <sup>-2</sup> )	Applied potential (V)	Refs.
PtW/MoS <sub>2</sub> /GCE	0.005	1.00 μM–0.20 mM	171.00	–0.25	[30]
AgNP–TiO <sub>2</sub> NWs/GCE	1.70	0.10 mM–60.00 mM	—	–0.30	[39]
PB–TiO <sub>2</sub> composite film/GCE	1.50	—	1726.8	–0.05	[40]
Au–Pd/MoS <sub>2</sub> /GCE	0.16	0.80 μM–10.00 mM	184.90	—	[41]
AuPd /C/GCE	8.40	—	195.30	0.25	[42]
Pt-IL-pGR/GCE	0.42	10.00μM–4.00 mM	942.15	0.074	[43]

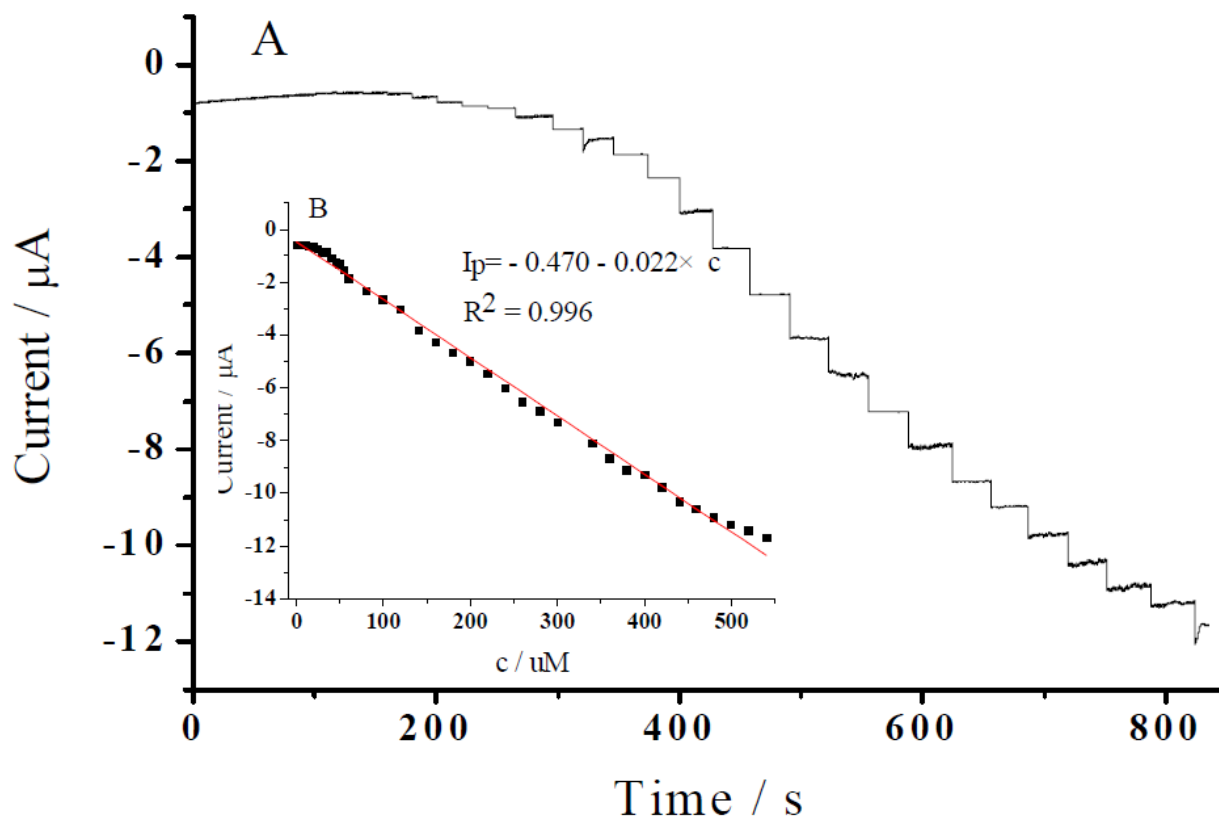


**Figure 9.** (A) Amperometric current response of the Au@Pd NPs/f-TiO<sub>2</sub>NTs/GCE on successive injection of H<sub>2</sub>O<sub>2</sub> into stirring N<sub>2</sub>-saturated PBS (pH 7.4) at an applied potential of 0.0 V. (B) Calibration curve for H<sub>2</sub>O<sub>2</sub> concentration from 1×10<sup>-7</sup> to 5×10<sup>-4</sup> M.

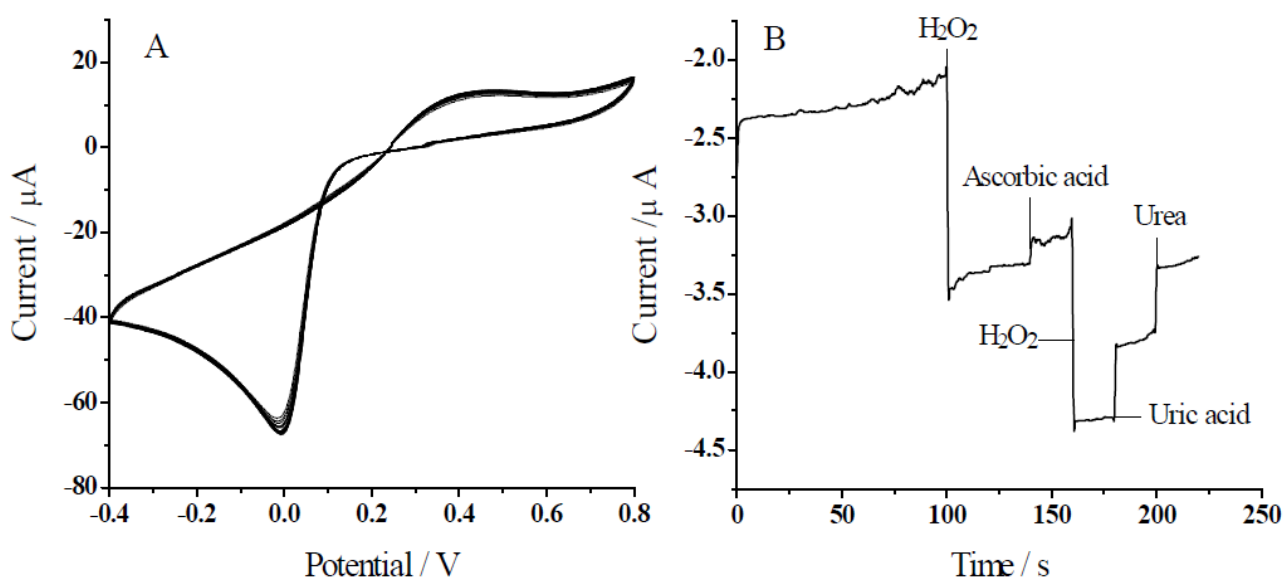


**Figure 10.** (A) CVs of H<sub>2</sub>O<sub>2</sub> reduction at the Au@Pd NPs/f-TiO<sub>2</sub>NTs/GCE in 0.1 M 20 mL PBS (pH 7.4) containing 0.5 mM H<sub>2</sub>O<sub>2</sub> for 20 consecutive cycles. (B) Amperometric responses of Au@Pd NPs/f-TiO<sub>2</sub>NTs/GCE upon subsequent additions of 0.05 mM H<sub>2</sub>O<sub>2</sub>, 0.5 mM AA, 0.05 mM H<sub>2</sub>O<sub>2</sub>, 0.5 mM UA and 0.5 mM Urea at 0.0 V.

To testify the reproducibility and stability of as-prepared Au@Pd NPs/f-TiO<sub>2</sub>NTs/GCE sensor, five Au@Pd NPs/f-TiO<sub>2</sub>NTs/GCEs were investigated in 0.5 mM H<sub>2</sub>O<sub>2</sub> at a scan rate of 50 mV/s. The relative standard deviation (R.S.D.) was 3.6%, confirming that the preparation method was highly reproducible. Stability of the modified electrode was tested by scanning the electrode continuously in 0.5 mM H<sub>2</sub>O<sub>2</sub>, and it was found that there was no apparent decrease in the current response for 20 consecutive cycles (Fig. 10A), which indicates that the fabricated Au@Pd NPs/f-TiO<sub>2</sub>NTs/GCE sensor had excellent stability. The selectivity of the f-TiO<sub>2</sub>NTs-Au@Pd/GCE for the detection of H<sub>2</sub>O<sub>2</sub> was also evaluated. Fig. 10B shows the current responses of 0.05 mM H<sub>2</sub>O<sub>2</sub>, 0.5 mM AA, 0.05 mM H<sub>2</sub>O<sub>2</sub>, 0.5 mM UA and 0.5 mM Urea on the Au@Pd NPs/f-TiO<sub>2</sub>NTs/GCE at 0.0 V. As seen, the current responses of AA, UA and Urea observed were much smaller than those of H<sub>2</sub>O<sub>2</sub>, indicating that the Au@Pd NPs/f-TiO<sub>2</sub>NTs/GCE has excellent selectivity for the detection of H<sub>2</sub>O<sub>2</sub>.

In order to evaluate the applicability of the proposed electrode, human blood serum sample was selected as real sample and detected with the optimal experimental procedure. In a typical procedure, the human serum was diluted 100 times with 0.10 M pH 7.4 PBS to fit the linear range of the proposed method and also reduce the matrix effect. In addition, to ascertain the correctness of the results, amperometric response was recorded after each addition of the standard H<sub>2</sub>O<sub>2</sub> solution at 0.0 V, the recovery was 95.96-106.21%. These results indicate that the prepared sensor is suitable for H<sub>2</sub>O<sub>2</sub> determination in real samples with a sufficient precision.

#### 4. CONCLUSIONS

In summary, a novel hybrid nanostructure with enhanced electrocatalytic performances was prepared by simple surface-modified method. Hybrid nanostructure was fabricated with assistance of APTMS, which acted as a linker. It was found that the as-prepared f-TiO<sub>2</sub>NTs is negatively charged in alkaline conditions as a result of the hydrolyzation of APTMS and offer versatile solid supports for Au@Pd NPs with opposite charge. The formation mechanism of such a composite nanostructure has been proposed, i.e., the -NH<sub>2</sub> groups of APTMS anchor to Au@Pd NPs with hydrogen bonds and metal-ligand coordination bonds, and the methoxy groups are available for the covalent linkage with abundant -OH groups from the surfaces of TiO<sub>2</sub>NTs. It is found that the fabricated non-enzymatic electrochemical sensor exhibited high electrocatalytic activity toward H<sub>2</sub>O<sub>2</sub> at low potential. The detection limit for H<sub>2</sub>O<sub>2</sub> is  $2 \times 10^{-8}$  M, which was lower than certain enzyme-based biosensors. Most importantly, this electrochemical sensor has high sensitivity for H<sub>2</sub>O<sub>2</sub>, and applied successfully to selective determination of H<sub>2</sub>O<sub>2</sub> in real sample with satisfactory recovery range.

#### ACKNOWLEDGMENTS

The authors gratefully acknowledge the financial support from International Cooperation Term of MOST, China (2009DFA32050), Fujian Department of Science and Technology (2008J0330, 2008F5033, 2009I0016), and Science Term of Fuzhou University (0460-023028), Yunnan Provincial Department of Education general Project (2013Y067), the National Science Foundation of China (NSFCs) (61361002, 20160906) and the Youth project of Yunnan Province (No 2014FD054).

## References

1. J.N. Gao, Y.J. He, X.Y. Zhao, X.Z. Ran, Y.H. Wu, Y.P. Su and J.W. Dai, *J. Colloid Interface Sci.*, 481 (2016) 220.
2. X.Y. Zhang, Q. Huang, M.Y. Liu, J.W. Tian, G.J. Zeng, Z. Li, K. Wang, Q.S. Zhang, Q. Wan, F. J. Deng and Y. Wei, *Appl. Surf. Sci.*, 343 (2015) 19.
3. M. Falahnejad, H. Zavvar Mousavi, H. Shir Khanloo and A.M. Rashidi, *Microchem. J.*, 125 (2016) 236.
4. L. Wu, L. Cai, A.Q. Liu, W. Wang, Y.H. Yuan and Z.X. Li, *Appl. Surf. Sci.*, 349 (2015) 683.
5. S.J. Limmer, T.P. Chou and G.Z. Cao, *J. Phys. Chem. B*, 107 (2003) 13313.
6. J. Lee, J.Y. Woo, J.T. Kim, B.Y. Lee and C.-S. Han, *ACS Appl. Mater. Interfaces*, 6 (2014) 10974.
7. S. J. Guo, J. Li, W. Ren, D. Wen, S. J. Dong, and E. K. Wang, *Chem. Mat.*, 21 (2009) 2247.
8. L. Hou, Z.Q. Gao, M.D. Xu, X. Cao, X.P. Wu, G.N. Chen and D.P. Tang, *Biosens. Bioelectron.*, 54 (2014) 365.
9. A. Navaee and A. Salimi, *Electrochim. Acta*, 211 (2016) 322.
10. H. Chakraborti and S.K. Pal, *Chem. Phys. Lett.*, 600 (2014) 118.
11. M.L. Zou, M.L. Dub, M. Zhang, T.T. Yang, H. Zhu, P. Wang and S.Y. Bao, *Mater. Res. Bull.*, 61 (2015) 375.
12. M. Nischk, P. Mazierski, Z.S. Wei, K. Siuzdak, N.A. Kouame, E. Kowalska, H. Remita and A. Zaleska-Medynska, *Appl. Surf. Sci.*, 387 (2016) 89.
13. X.H. Huo, P.P. Liu, J. Zhu, X.Q. Liu and H.X. Ju, *Biosens. Bioelectron.*, 85 (2016) 698.
14. G.W. Zhang, H. Miao, X.Y. Hua, J.L. Mu, X.X. Liu, T.X. Han, J. Fan, E.Z. Liu, Y.C. Yin and J. Wan, *Appl. Surf. Sci.*, xxx (2016) xxx.
15. H.B. Yu, X.H. Wang, H.W. Sun and M.X. Huo, *J. Hazard. Mater.*, 184 (2010) 753.
16. X. Yang, W.B. Wang, L.P. Wu, X.J. Lia, T.J. Wang and S.J. Liao, *Appl. Catal.*, A 526 (2016) 45.
17. A.H. Liu, M.D. Wei, I. Honma and H.S. Zhou, *Adv. Funct. Mater.*, 16 (2006) 371.
18. A. Ayati, B. Tanhaei, F.F. Bamoharram, A. Ahmadpour, P. Maydannik and M. Sillanpää, *Sep. Purif. Technol.*, 171 (2016) 62.
19. L.X. Wang, C.G. Hu, Y. Zhao, Y. Hu, F. Zhao, N. Chen and L.T. Qu, *Carbon*, 74 (2014) 170.
20. Y.J. Ma, H. Li, H. Wang, X.F. Mao, V. Linkov, S. Ji, O.U. Gcilitshana and R.F. Wang, *J. Power Sources*, 268 (2014) 498.
21. H.J. Zhang and N. Toshima, *J. Colloid Interface Sci.*, 394 (2013) 166.
22. Y. Mizukoshia, K. Satob, T.J. Konnob and N. Masahashi, *Appl. Catal. B: Environ*, 94 (2010) 248.
23. A. Villa, N. Janjic, P. Spontoni, D. Wang, D.S. Su and L. Prati, *Appl. Catal.*, A 364 (2009) 221.
24. Y.W. Lee, N.H. Kim, K.Y. Lee, K. Kwon, M. Kim and S.W. Han, *J. Phys. Chem. C*, 112 (2008) 6717.
25. X.L. Chen, H.B. Pan, H.F. Liu and M. Du, *Electrochim. Acta*, 56 (2010) 636.
26. W.X. Yin, Z.P. Li, J.K. Zhu and H.Y. Qin, *J. Power Sources*, 182 (2008) 520.
27. T. Sreethawong and S. Yoshikawa, *Int. J. Hydrogen Energy*, 31 (2006) 786.
28. A. Sarkany, P. Hargittai and A. Horvath, *Top. Catal.*, 46 (2007) 121.
29. M.J. Zhu, M.Z. Lerum and W. Chen, *Langmuir*, 28 (2012) 416.
30. D.L. Jiang, Y. Zhang, M.H. Huang, J. Liu, J. Wan, H.Y. Chu and M. Chen, *J. Electroanal. Chem.*, 728 (2014) 26.
31. L.L. Zhu, Y. Zhang, P.Z. Xu, W. J. Wen, X.X. Li and J.Q. Xu, *Biosens. Bioelectron.*, 80 (2016) 601.
32. X.D. Zeng, X.Y. Liu, B. Kong, Y. Wang and W.Z. Wei, *Sensors Actuat. B*, 133 (2008) 381.
33. S.H. Lim, J. Luo, Z. Zhong, W. Ji and J. Lin, *Inorg. Chem.*, 44 (2005) 4124.
34. H.-H. Ou and S.-L. Lo, *Sep. Purif. Technol.*, 58 (2007) 179.
35. G. Demirel, M. Çakmak, T. Çaykara and Ş. Ellialtıoğlu, *J. Phys. Chem. C*, 111 (2007) 15020.
36. X.L. Chen, W. Liu, L.L. Tang, J. Wang, H.B. Pan and M. Du, *Mater. Sci. Eng. C*, 34 (2014) 304.

37. J.-W. Hu, J.-F. Li, B. Ren, D.-Y. Wu, S.-G. Sun and Z.-Q. Tian, *J. Phys. Chem. C*, 111 (2007) 1105.
38. A. Villa, N. Janjic, P. Spontoni, D. Wang, D.S. Su and L. Prati, *Appl. Catal., A*, 364 (2009) 221.
39. X.Y. Qin, W. B. Lu, Y.L. Luo, G.H. Chang, A.M. Asiri, A.O. Al-Youbi and X.P. Sun, *Electrochim. Acta*, 74 (2012) 275.
40. Z.Y. Chu, L. Shi, Y. Liu, W.Q. Jin and N.P. Xu, *Biosens. Bioelectron.*, 47 (2013) 329.
41. X.Y. Li and X.Z. Du, *Sens. Actuators, B*, 239 (2017) 536.
42. T.T. Han, Y. Zhang, J.Q. Xua, J.P. Dong and C.-C. Liu, *Sens. Actuators, B*, 207 (2015) 404.
43. H.S. Zhang, X.J. Bo and L.P. Guo, *Electrochim. Acta*, 201 (2016) 117.

© 2017 The Authors. Published by ESG ([www.electrochemsci.org](http://www.electrochemsci.org)). This article is an open access article distributed under the terms and conditions of the Creative Commons Attribution license (<http://creativecommons.org/licenses/by/4.0/>).